JOURNAL OF GUIDANCE, CONTROL, AND DYNAMICS
Vol. 31, No. 4, July–August 2008

Decentralized Cooperative-Control Design for Multivehicle Formations

Lesley A. Weitz* and John E. Hurtado†
Texas A&M University, College Station, Texas 77843
and
Andrew J. Sinclair‡
Auburn University, Auburn, Alabama 36849

DOI: 10.2514/1.33009

In a decentralized cooperative-control regime, individual vehicles autonomously compute their required control inputs to achieve a group objective. Controlling formations of individual vehicles is one application of decentralized cooperative control. In this paper, cooperative-control schemes are developed for a multivehicle formation problem with information flow modeled by leader–follower subsystems. Control laws are developed to drive position and velocity errors between vehicle pairs to zero. The general control law for the *i*th vehicle tracks its lead vehicle's position and velocity, as well as a reference position and velocity that the whole formation follows. Rate-estimation schemes are developed for the general control law using both Luenberger-observer and passive-filtering estimation methods. It is shown that these estimation methods are complicated by the effects that the estimated rates have on formation stability. Finally, the development of a rate-free controller is presented, which does not require state information from other vehicles in the formation. The control schemes are simulated for a five-vehicle formation and are compared for stability and formation convergence.

I. Introduction

COOPERATIVE control involves the control of a group of entities that are working collectively to meet a common objective. This is an emerging area of research with widespread application to problems in several engineering disciplines. The basis of a cooperative-control scheme lies within the ability to take state information from individual entities and their surrounding environments for use in determining appropriate control inputs to the different vehicles. Understanding the dynamic behavior that governs these entities is key to designing cooperative-control laws that will influence how entities interact to achieve a desired goal.

Decentralized cooperative control is a subset of cooperative control in which vehicles share information with other vehicles and autonomously determine their own control inputs to achieve a group objective. In many applications, the entities only communicate with their nearest neighbors, rather than with all vehicles in a system. A decentralized-control regime is typically considered superior to more traditional centralized controllers; a central control authority would use state and environmental information to determine the control inputs for each individual vehicle. This is an effective method for controlling a small number of vehicles, but centralized control becomes computationally inefficient as the number of entities gets larger. Moreover, decentralization is more robust to communication failures and structural reconfigurations [1].

Some of the research in the area of decentralized cooperative systems has focused on formation control, and this research has varied greatly. Feddema et al. [2] demonstrate the applicability of decentralized-control theory to cooperative robotic vehicles to achieve a desired formation. In that paper, they address whether large-scale decentralized techniques can be used to control multiple robotic vehicles when the system is modeled as a large-dimensional interconnected system. Other solutions to the vehicle-formation problem have included using dynamic inversion [3] or structural potential functions [4].

One particular path for vehicle formation-control research was to develop control laws for overlapping subsystems. Formations can be modeled as interconnected and overlapping subsystems, due to the common leader–follower information structure in vehicle formations. The underlying concept for controller design is the ability to expand the overlapping systems into a higher-dimensional space in which the subsystems appear to be decoupled. The controllers are then designed in the expanded space and contracted back to the original space for implementation [5–7]. Stipanović et al. [8] used this method to design cooperative control laws for a planar unmanned-aerial-vehicle (UAV) formation.

In this paper, control-law design and stability of multivehicle formations is explored. We take advantage of the differential-flatness property of a commonly used nonlinear vehicle model, which allows the vehicle motion to be described using a linear form [9–11]. The control-law design is then approached from an error-dynamics perspective in which the form of the vehicle model is exploited to formulate error variables between neighboring vehicles in the formation. In addition to the control-law design, two rate-estimation techniques are explored. Using rate estimates complicates the nonlinear-to-linear model transformation, and stability is difficult to analyze. To deal with this problem, rate-estimation equations are designed using the linear-model representation and then formation stability is explored using simulation results. Finally, a rate-free control law is designed, which does not require state information from other vehicles in the formation to implement.

The major contributions of this paper are the straightforward formation-control design for an accelerating formation using the linear form of the vehicle model; the exploration of the rate-estimation techniques and challenges associated with the nonlinear model; the rate-free control-law development, including an asymptotic stability proof of the rate-free control law using Lyapunov theory; and, finally, the comparison of these control techniques for a multivehicle formation. Section II of the paper

Received 22 June 2007; revision received 16 January 2008; accepted for publication 19 February 2008.

*Graduate Student, Department of Aerospace Engineering, 3141 TAMU; lweitz@tamu.edu. Member AIAA.
†Associate Professor, Department of Aerospace Engineering, 3141 TAMU; jehurtado@tamu.edu. Senior Member AIAA.
‡Assistant Professor, Department of Aerospace Engineering, 211 Aerospace Engineering Building; sinclair@auburn.edu. Member AIAA.

describes the nonlinear vehicle model and the differential-flatness property that enables the nonlinear-model transformation to a linear form. Section III presents the development of the general controller, including the form of the system error dynamics, and rate-estimation techniques are presented in Sec. IV. The development of the rate-free controller is in Sec. V. Simulation results using both the simple nonlinear model and a six-degree-of-freedom UAV model are presented in Sec. VI, followed by conclusions in Sec. VII.

II. Vehicle Model

In this section, a commonly used nonlinear kinematics model is presented that represents a vehicle with zero or negligible velocity in the direction perpendicular to the vehicle's heading.

$$\dot{x} = v\cos\psi; \qquad \dot{y} = v\sin\psi; \qquad \dot{\psi} = \omega \tag{1}$$

where x and y are the vehicle's position in the 2-D plane, v is the velocity in the direction of motion, ψ is the heading angle relative to the x axis, and ω is the angular turn rate of the vehicle. The velocity and angular turn rate are assumed to be the control inputs to the vehicle. Figure 1 shows the vehicle position and orientation in the inertial reference frame.

The vehicle model in Eq. (1) is an underactuated system with three states and two controls. However, the vehicle model is affine in control with codimension one (three states and two controls), and thus the model is differentially flat, with flat outputs x and y [12]. As a result of the differential-flatness property, the state ψ and the two control inputs can be written as functions of the flat outputs and their derivatives, as shown next.

$$v = \sqrt{\dot{x}^2 + \dot{y}^2}; \qquad \psi = \tan^{-1}\left(\frac{\dot{y}}{\dot{x}}\right); \qquad \omega = \frac{\ddot{y}\dot{x} - \dot{y}\ddot{x}}{v^2} \tag{2}$$

The second derivatives of the flat outputs are the highest derivatives that appear in the controls v and ω. Therefore, new control inputs can be defined as $(\ddot{x}, \ddot{y}) = (u, w)$. This transformation enables the nonlinear system in Eq. (1) to be represented as uncoupled double integrators.

$$\begin{bmatrix} \dot{x} \\ \dot{y} \\ \ddot{x} \\ \ddot{y} \end{bmatrix} = \begin{bmatrix} 0 & 0 & 1 & 0 \\ 0 & 0 & 0 & 1 \\ 0 & 0 & 0 & 0 \\ 0 & 0 & 0 & 0 \end{bmatrix} \begin{bmatrix} x \\ y \\ \dot{x} \\ \dot{y} \end{bmatrix} + \begin{bmatrix} 0 & 0 \\ 0 & 0 \\ 1 & 0 \\ 0 & 1 \end{bmatrix} \begin{bmatrix} u \\ w \end{bmatrix} \tag{3}$$

Thus, the control-law design is made easier by the transformation to the linear representation. It should be noted that Eq. (3) is not a linear approximation of the nonlinear vehicle model, but an exact linear representation. The behavior of the differentially flat system enables the design of arbitrary trajectories in the flat-output (x, y) space, which can then be mapped to the appropriate inputs, as indicated in Eq. (2) [13].

III. Control-Law Development

In this paper, we focus on a leader–follower communication structure for the decentralized formation-control problem. Figure 2 shows a five-vehicle formation in which each leader–follower vehicle pair is denoted by the dashed lines, and communication flow is shown by the arrows between vehicles. For example, V_2 receives state information from its lead V_1, and V_3 receives information from V_2. V_1 will be referred to as the formation lead. Figure 2 shows two vehicle platoons; the formation-control laws for each platoon can be implemented independently. The vehicle indices in the next development are consistent with platoon 1; however, all development is also applicable to platoon 2.

The design focus is on the internal stability of the formation (i.e., the ability to achieve and maintain a desired formation). The control laws are developed by defining error variables between the leader–follower vehicle pairs, as shown next. The defined errors are in the x direction only. Because of the uncoupled nature of the equations of motion, the development is identical in the y direction.

$$e_1 = x_r - x_1 - d_1; \quad \dot{e}_1 = \dot{x}_r - \dot{x}_1; \quad \ddot{e}_1 = \ddot{x}_r - \ddot{x}_1 = \ddot{x}_r - u_1 \tag{4a}$$

$$e_2 = x_1 - x_2 - d_2; \quad \dot{e}_2 = \dot{x}_1 - \dot{x}_2; \quad \ddot{e}_2 = \ddot{x}_1 - \ddot{x}_2 = u_1 - u_2 \quad \cdots \tag{4b}$$

$$e_i = x_{i-1} - x_i - d_i; \quad \dot{e}_i = \dot{x}_{i-1} - \dot{x}_i; \quad \ddot{e}_i = \ddot{x}_{i-1} - \ddot{x}_i = u_{i-1} - u_i \tag{4c}$$

The formation lead tracks a reference trajectory x_r at some constant distance d_1, as denoted by the e_1 equation; e_2 is the relative error between vehicles 1 and 2 separated by some constant distance d_2; and the error equations can be generalized for the ith vehicle, as already shown.

The control objective is to design control inputs u_i that stabilize the error dynamics for a system of n vehicles described by the differential equation $\dot{\mathbf{e}} = A\mathbf{e} + B\mathbf{U}$.

$$\begin{aligned} \mathbf{e} &= \begin{bmatrix} e_1 & \dot{e}_1 & e_2 & \dot{e}_2 & \cdots & e_n & \dot{e}_n \end{bmatrix}^T; \\ \mathbf{U} &= \begin{bmatrix} \ddot{x}_r & u_1 & u_2 & \cdots & u_n \end{bmatrix}^T = \begin{bmatrix} \ddot{x}_r & \mathbf{u} \end{bmatrix}^T \end{aligned} \tag{5}$$

$$A = \begin{bmatrix} 0 & 1 & 0 & 0 & \cdots & 0 & 0 \\ 0 & 0 & 0 & 0 & \cdots & 0 & 0 \\ 0 & 0 & 0 & 1 & \cdots & 0 & 0 \\ 0 & 0 & 0 & 0 & \cdots & 0 & 0 \\ \vdots & \vdots & \vdots & \vdots & \ddots & \vdots & \vdots \\ 0 & 0 & 0 & 0 & \cdots & 0 & 1 \\ 0 & 0 & 0 & 0 & \cdots & 0 & 0 \end{bmatrix};$$

$$B = \begin{bmatrix} 0 & 0 & 0 & \cdots & 0 & 0 \\ 1 & -1 & 0 & \cdots & 0 & 0 \\ 0 & 0 & 0 & \cdots & 0 & 0 \\ 0 & 1 & -1 & \cdots & 0 & 0 \\ \vdots & \vdots & \vdots & \ddots & \vdots & \vdots \\ 0 & 0 & 0 & \cdots & 0 & 0 \\ 0 & 0 & 0 & \cdots & 1 & -1 \end{bmatrix} \tag{6}$$

where A is a $2n \times 2n$ matrix, and B is a $2n \times (n+1)$ matrix.

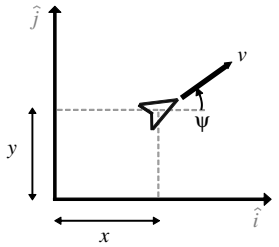

Fig. 1 Vehicle position and orientation in the *x*–*y* plane.

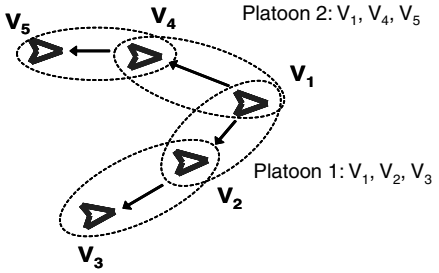

Fig. 2 Leader–follower communication structure for a multivehicle formation [8].

The following form is assumed for the control inputs u_i.

$$\mathbf{u} = \begin{bmatrix} k_{p_1} & k_{v_1} & 0 & 0 & \cdots & 0 & 0 \\ 0 & 0 & k_{p_2} & k_{v_2} & \cdots & 0 & 0 \\ \vdots & \vdots & \vdots & \vdots & \ddots & \vdots & \vdots \\ 0 & 0 & 0 & 0 & \cdots & k_{p_n} & k_{v_n} \end{bmatrix} \mathbf{e} + \begin{bmatrix} c_{p_1} & c_{v_1} & 0 & 0 & \cdots & 0 & 0 \\ c_{p_2} & c_{v_2} & c_{p_2} & c_{v_2} & \cdots & 0 & 0 \\ \vdots & \vdots & \vdots & \vdots & \ddots & \vdots & \vdots \\ c_{p_n} & c_{v_n} & c_{p_n} & c_{v_n} & \cdots & c_{p_n} & c_{v_n} \end{bmatrix} \mathbf{e} + \ddot{x}_r \tag{7}$$

The ith control law can be generalized, and the terms are expanded using the definitions for the error terms in Eq. (4).

$$\begin{aligned} u_i &= k_{p_i} e_i + k_{v_i} \dot{e}_i + c_{p_i}(e_1 + e_2 + \cdots + e_i) \\ &\quad + c_{v_i}(\dot{e}_1 + \dot{e}_2 + \cdots + \dot{e}_i) + \ddot{x}_r = k_{p_i}(x_{i-1} - x_i - d_i) \\ &\quad + k_{v_i}(\dot{x}_{i-1} - \dot{x}_i) + c_{p_i}\left(x_r - x_i - \sum_{j=1}^{i} d_j\right) \\ &\quad + c_{v_i}(\dot{x}_r - \dot{x}_i) + \ddot{x}_r \end{aligned} \tag{8}$$

Because of the selected leader–follower communication structure, the homogeneous error dynamics always have a lower-diagonal block form. The closed-loop characteristic polynomial can then be determined from the diagonal blocks. Therefore, the characteristic polynomial of the closed-loop error dynamics has the following form, and the equivalent eigenvalues are easily found.

$$\begin{aligned} &\prod_{i=1}^{n}[s^2 + (k_{v_i} + c_{v_i})s + (k_{p_i} + c_{p_i})] = 0 \\ &\Rightarrow \lambda_{i_{1,2}} = -\frac{(k_{v_i} + c_{v_i})}{2} \pm \frac{\sqrt{(k_{v_i} + c_{v_i})^2 - 4(k_{p_i} + c_{p_i})}}{2} \end{aligned} \tag{9}$$

Based upon the form of the general control law in Eq. (8), some specific control-gain choices are presented here.

1) For case 1, $k_p, k_v \neq 0$ and $c_p, c_v = 0$. For this choice of gains, each vehicle tracks its lead vehicle's position and velocity.

2) For case 2, $k_p, k_v = 0$ and $c_p, c_v \neq 0$. In this case, each vehicle tracks the reference position and velocity of the formation leader, rather than its assigned lead vehicle's position and velocity. Therefore, it would be assumed in this case that each vehicle knows the reference trajectory of the formation lead, as well as its desired separation from the reference trajectory.

3) For case 3, $k_p, k_v, c_v \neq 0$ and $c_p = 0$. Case 3 combines some of the behaviors in the previous two cases: the ith vehicle tracks its lead's position and velocity and the reference velocity.

4) For case 4, $k_p, k_v, c_p, c_v \neq 0$. In this case, the control law combines both reference-trajectory and lead-vehicle tracking schemes.

Case 4 leads to both lead-vehicle and reference-trajectory tracking strategies in which the gains are chosen based upon the desired weighting of each strategy. Case 1 may be used if the reference trajectory is not known by all vehicles in the formation, whereas case 2 may be chosen if lead-vehicle information is unavailable.

IV. Rate Estimation

The previous control-law developments require both position and rate information from the ith vehicle. In addition, position and rate information from the assigned lead-vehicle and reference-trajectory position and rate information are required for control implementation in case 4. In this section, we explore control-law implementation without direct measurements of vehicle rates $\dot{x}$ and $\dot{y}$. In many aerospace applications, full-state measurement eliminates the need for rate estimation, but our interest in this development stems from vehicle applications with limited sensor packages, such as small robotic vehicles or inexpensive, easily deployable UAVs.

When rates are known, the computation of the control inputs in the nonlinear form is straightforward using u and w from the linear control design. However, this relationship is complicated if rates are unknown. If the vehicle velocity v is a state in the nonlinear vehicle representation in Eq. (1), then $\dot{v}$ can be considered to be a control input that describes the behavior of v. A linear transformation T relates the control inputs for the nonlinear representation $\dot{v}$ and ω to u and w.

$$\begin{bmatrix} \dot{v} \\ \omega \end{bmatrix} = \frac{1}{v}\begin{bmatrix} \dot{x} & \dot{y} \\ -\frac{\dot{y}}{v} & \frac{\dot{x}}{v} \end{bmatrix}\begin{bmatrix} u \\ w \end{bmatrix} = T(\dot{x}, \dot{y})\begin{bmatrix} u \\ w \end{bmatrix}; \qquad v = \sqrt{\dot{x}^2 + \dot{y}^2} \tag{10}$$

However, when rate estimates for $\dot{x}$ and $\dot{y}$, denoted as $\dot{\hat{x}}$ and $\dot{\hat{y}}$, are used to compute the original controls, estimation dynamics are added to the system response, as shown next.

$$\begin{bmatrix} \dot{v} \\ \omega \end{bmatrix} = \frac{1}{\hat{v}}\begin{bmatrix} \dot{\hat{x}} & \dot{\hat{y}} \\ -\frac{\dot{\hat{y}}}{\hat{v}} & \frac{\dot{\hat{x}}}{\hat{v}} \end{bmatrix}\begin{bmatrix} u \\ w \end{bmatrix} = T(\dot{\hat{x}}, \dot{\hat{y}})\begin{bmatrix} u \\ w \end{bmatrix}; \qquad \hat{v} = \sqrt{\dot{\hat{x}}^2 + \dot{\hat{y}}^2} \tag{11}$$

From a first-order linearization of $T(\dot{\hat{x}}, \dot{\hat{y}})$ about $\dot{x}$ and $\dot{y}$, it can be seen that a rate-estimation scheme adds error terms to the control transformation. These error terms are related to the errors between the actual and estimated rates.

$$\begin{aligned} T(\dot{\hat{x}}, \dot{\hat{y}}) &\approx T(\dot{x}, \dot{y}) + \left.\frac{\partial T}{\partial \dot{\hat{x}}}\right|_{\dot{x}} (\dot{\hat{x}} - \dot{x}) + \left.\frac{\partial T}{\partial \dot{\hat{y}}}\right|_{\dot{y}} (\dot{\hat{y}} - \dot{y}) \approx T(\dot{x}, \dot{y}) \\ &\quad + \begin{bmatrix} \frac{1}{v} - \frac{\dot{x}^2}{v^3} & -\frac{\dot{y}\dot{x}}{v^3} \\ \frac{2\dot{y}\dot{x}}{v^4} & \frac{1}{v^2} - \frac{2\dot{x}^2}{v^4} \end{bmatrix}(\dot{\hat{x}} - \dot{x}) + \begin{bmatrix} -\frac{\dot{x}\dot{y}}{v^3} & \frac{1}{v} - \frac{\dot{y}^2}{v^3} \\ -\frac{1}{v^2} + \frac{2\dot{y}^2}{v^4} & -\frac{2\dot{x}\dot{y}}{v^4} \end{bmatrix}(\dot{\hat{y}} - \dot{y}) \end{aligned} \tag{12}$$

These rate-estimation errors are amplified through the Jacobian of the transformation evaluated at the true rates. Because the stability of the preceding transformation is difficult to determine analytically, rate-estimation schemes are designed using the double-integrator model in Eq. (3). System stability is then evaluated using simulation results for the nonlinear system using the control transformation with rate estimates in Eq. (11).

Vehicle rate estimation is explored in two ways: first, a Luenberger-observer method is presented, which is a straightforward derivation, given the linear vehicle model and the control-law form described in Eq. (8); second, a first-order passive filter of the position states is explored.

A. Luenberger Observer

Rate estimation using a Luenberger observer [14] is an alternative to measuring all required states using onboard sensing. The general control law for the ith vehicle in Eq. (8) requires the following state information: x_i, $\dot{x}_i$, x_{i-1}, $\dot{x}_{i-1}$, x_r, and $\dot{x}_r$. Our objective is to estimate the vehicle rates $\dot{x}_i$ and $\dot{x}_{i-1}$, which will be denoted as $\dot{\hat{x}}_i$ and $\dot{\hat{x}}_{i-1}$, respectively. In addition, it is assumed that the $(i-1)$th vehicle communicates its own rate estimate to the ith vehicle. Note that estimating the rate of the $(i-1)$th vehicle onboard the ith vehicle would not meet the leader–follower communication structure that was previously defined, because the ith vehicle would then need state information from all of the preceding vehicles to implement the observer.

The closed-loop equations of motion for the ith vehicle are next described in matrix form for full-state knowledge.

$$\begin{bmatrix}\dot{x}_i\\ \ddot{x}_i\end{bmatrix}=\left(\begin{bmatrix}0 & 1\\ -(k_{p_i}+c_{p_i}) & 0\end{bmatrix}+\begin{bmatrix}0 & 0\\ 0 & -(k_{v_i}+c_{v_i})\end{bmatrix}\right)\begin{bmatrix}x_i\\ \dot{x}_i\end{bmatrix}+\begin{bmatrix}0 & 0\\ k_{p_i} & k_{v_i}\end{bmatrix}\begin{bmatrix}x_{i-1}\\ \dot{\hat{x}}_{i-1}\end{bmatrix}+\begin{bmatrix}0 & 0 & 0\\ c_{p_i} & c_{v_i} & 1\end{bmatrix}\begin{bmatrix}x_r\\ \dot{x}_r\\ \ddot{x}_r\end{bmatrix}+\begin{bmatrix}0\\ -k_{p_i}d_i-c_{p_i}\sum_{j=1}^{i}\mathrm{d}_j\end{bmatrix} \tag{13}$$

Equation (13) is rewritten in the following matrix notation.

$$\dot{\mathbf{x}}_i=(A_1+A_2)\mathbf{x}_i+B_1\mathbf{x}_{\mathrm{i}}+B_2\mathbf{x}_{\mathrm{r}}+B_3 \tag{14}$$

where the A_1 matrix represents the kinematics and contains the position gains from the control law, and A_2 contains the velocity gains. The A_1 and A_2 matrices are divided into terms that will act on known states and terms that will act on estimated states. The B_1 matrix is the input matrix from the $(i-1)$th vehicle, the B_2 matrix is the input matrix for the reference-trajectory states, and the B_3 matrix represents the distances of the ith vehicle from both its lead vehicle and the reference trajectory. The vectors in this matrix representation are defined as $\mathbf{x}_{\mathrm{i}}=[x_i,\dot{x}_i]^T$, $\mathbf{x}_{\mathrm{i-1}}=[x_{i-1},\dot{\hat{x}}_{i-1}]^T$, and $\mathbf{x}_{\mathrm{r}}=[x_r,\dot{x}_r,\ddot{x}_r]^T$.

In developing the state estimator for the ith vehicle, it is assumed that the vehicle position is known and the measured position x_{i_m} can be represented by a linear equation.

$$x_{i_m}=C\mathbf{x}_{\mathrm{i}};\qquad C=\begin{bmatrix}1 & 0\end{bmatrix} \tag{15}$$

Then the closed-loop estimator can be written by replacing $\mathbf{x}_{\mathrm{i}}$ with $\hat{\mathbf{x}}_i$ and by adding an error term between the estimated and the measured quantities. The estimation-gain matrix L_i is selected to drive the estimated states to the actual states.

$$\begin{aligned}\dot{\hat{\mathbf{x}}}_i&=(A_1+A_2)\hat{\mathbf{x}}_i+B_1\mathbf{x}_{\mathrm{i-1}}+B_2\mathbf{x}_r+B_3+L_i(x_{i_m}-C\hat{\mathbf{x}}_i)\\&=(A_1+A_2-L_iC)\hat{\mathbf{x}}_i+B_1\mathbf{x}_{\mathrm{i-1}}+B_2\mathbf{x}_r+B_3+L_iC\mathbf{x}_i\end{aligned} \tag{16}$$

From Eqs. (14) and (16), the equations for the feedback system to estimate both x_i and $\dot{x}_i$ can be determined; the rate estimate $\dot{\hat{x}}_i$ is used in place of $\dot{x}_i$ in the feedback control law. The overall system of equations for the ith vehicle has the following form.

$$\begin{bmatrix}\dot{\mathbf{x}}_i\\ \dot{\hat{\mathbf{x}}}_i\end{bmatrix}=\begin{bmatrix}A_1 & A_2\\ L_iC & A_1+A_2-L_iC\end{bmatrix}\begin{bmatrix}\mathbf{x}_i\\ \hat{\mathbf{x}}_i\end{bmatrix}+\begin{bmatrix}B_1\\ B_1\end{bmatrix}\mathbf{x}_{\mathrm{i-1}}+\begin{bmatrix}B_2\\ B_2\end{bmatrix}\mathbf{x}_r+\begin{bmatrix}B_3\\ B_3\end{bmatrix} \tag{17}$$

Note that only the kinematics term in the matrix A_1 acts on $\dot{x}_i$, and the position-gain term acts on x_i, which is known. The matrix A_2 only acts on the rate term in $\hat{\mathbf{x}}_i$, which is an estimated quantity. The top row of Eq. (17) represents the vehicle dynamics responding to the control input with estimated rates, and the bottom row is the onboard filter that determines the estimated states.

The stability of the closed-loop control law with the filter in Eq. (17) can be evaluated using the eigenvalues of the matrix that acts on $[\mathbf{x}_i,\hat{\mathbf{x}}_i]^T$. Stability is achieved if the estimation-gain matrix L_i is chosen such that the estimation filter is faster than the closed-loop dynamics. The eigenvalues for the overall system of n vehicles are equal to the union of the eigenvalues of each individual vehicle system, as shown in Eq. (17). The system eigenvalues are shown next.

$$\begin{aligned}\lambda_{i_{1,2}}&=\frac{-(k_{v_i}+c_{v_i})}{2}\pm\frac{\sqrt{(k_{v_i}+c_{v_i})^2-4(k_{p_i}+c_{p_i})}}{2};\\ \lambda_{i_{3,4}}&=\frac{-L_{i_1}}{2}\pm\frac{\sqrt{L_{i_1}^2-4(k_{p_i}+c_{p_i}+L_{i_2})}}{2};\qquad L_i=[L_{i_1}L_{i_2}]^T\end{aligned} \tag{18}$$

Thus, the rate-estimation scheme leads to the following general control form.

$$\begin{aligned}u_i&=k_{p_i}(x_{i-1}-x_i-d_i)+k_{v_i}(\dot{\hat{x}}_{i-1}-\dot{\hat{x}}_i)\\&\quad+c_{p_i}\left(x_r-x_i-\sum_{j=1}^{i}\mathrm{d}_j\right)+c_{v_i}(\dot{x}_r-\dot{\hat{x}}_i)\end{aligned} \tag{19}$$

When there is no error in the initial-rate estimates (i.e., the estimated and true rates are equal at time zero), the formation behavior is identical to the behavior with known states, because the Luenberger observer is an exact estimate of the closed-loop vehicle response.

B. Passivity Filter

Using a passivity filter is another method for estimating rate information. There are several examples in the literature of using passive filters to estimate rate information for control of robotic manipulators and attitude stabilization [15–17]. These concepts are used here to develop an expression to estimate vehicle rates. The passive filter has the form shown next, where the vehicle position is filtered using a fictitious state ϕ_i.

$$\dot{\phi}_i=-\tau_i\phi_i+k_ix_i \tag{20}$$

The position x_i in the filter equation is equivalent to a function of the reference trajectory and position errors:

$$x_i=x_r-e_1-e_2-\cdots-e_i-\sum_{j=1}^{i}\mathrm{d}_j$$

When the n-vehicle formation has reached its desired formation, all of the spacing errors e_i are zero and

$$x_i=x_r-\sum_{j=1}^{i}\mathrm{d}_j$$

Assuming that x_r has a constant acceleration, we can substitute

$$x_i=\frac{1}{2}\ddot{x}_rt^2+\dot{x}_r(0)t-\sum_{j=1}^{i}\mathrm{d}_j$$

and a solution for $\phi_i(t)$ can be found.

$$\begin{aligned}\phi_i(t)&=Ce^{-\tau_it}+\frac{k_i}{2\tau_i}\ddot{x}_rt^2+\left(\frac{k_i\dot{x}_r(0)}{\tau_i}-\frac{k_i}{\tau_i^2}\ddot{x}_r\right)t\\&\quad+\left(-\frac{k_i\sum_{j=1}^{i}\mathrm{d}_j}{\tau_i}-\frac{k_i\dot{x}_r(0)}{\tau_i^2}+\frac{k_i}{\tau_i^3}\ddot{x}_r\right)=Ce^{-\tau_it}\\&\quad+\frac{k_i}{\tau_i}\left(\frac{1}{2}\ddot{x}_rt^2+\dot{x}_r(0)t-\sum_{j=1}^{i}\mathrm{d}_j\right)-\frac{k_i}{\tau_i^2}(\ddot{x}_rt+\dot{x}_r(0))\\&\quad+\frac{k_i}{\tau_i^3}\ddot{x}_r=Ce^{-\tau_it}+\frac{k_i}{\tau_i}x_i-\frac{k_i}{\tau_i^2}\dot{x}_r+\frac{k_i}{\tau_i^3}\ddot{x}_r\end{aligned} \tag{21}$$

As t becomes large, $Ce^{-\tau_it}$ becomes small; thus, this term can be neglected. The reference velocity $\dot{x}_r$ is equal to $\dot{x}_i$ when the position errors have gone to zero, and because ϕ_i lags x_i, the next equation is an estimate of $\dot{x}_i$.

$$\dot{\hat{x}}_i\approx\dot{x}_r=\tau_ix_i-\frac{\tau_i^2}{k_i}\phi_i+\frac{1}{\tau_i}\ddot{x}_r \tag{22}$$

As was the case in the Luenberger-observer design, the passivity filters can be designed for the individual vehicles, and the overall system stability is guaranteed, given individual vehicle stability. The next equation shows the closed-loop state and passivity-filter equations for the ith vehicle, where $\dot{x}_i$ was replaced with Eq. (22).

$$\begin{bmatrix} \dot{x}_i \\ \ddot{x}_i \\ \dot{\phi}_i \end{bmatrix} = \begin{bmatrix} 0 & 1 & 0 \\ -(k_{p_i} + c_{p_i}) - \tau_i(k_{v_i} + c_{v_i}) & 0 & \frac{\tau_i^2}{k_i}(k_{v_i} + c_{v_i}) \\ k_i & 0 & -\tau_i \end{bmatrix} \begin{bmatrix} x_i \\ \dot{x}_i \\ \phi_i \end{bmatrix} + \begin{bmatrix} 0 & 0 \\ k_{p_i} & k_{v_i} \\ 0 & 0 \end{bmatrix} \begin{bmatrix} x_{i-1} \\ \dot{x}_{i-1} \end{bmatrix} + \begin{bmatrix} 0 & 0 & 0 \\ c_{p_i} & c_{v_i} & 1 - \frac{(k_{v_i} + c_{v_i})}{\tau_i} \\ 0 & 0 & 0 \end{bmatrix} \begin{bmatrix} x_r \\ \dot{x}_r \\ \ddot{x}_r \end{bmatrix} + \begin{bmatrix} 0 \\ -k_{p_i} d_i - c_{p_i} \sum_{j=1}^{i} \mathrm{d}_j \\ 0 \end{bmatrix} \tag{23}$$

The eigenvalues of Eq. (23) do not have a concise analytical form; however, the characteristic equation is

$$s^3 + \tau_i s^2 + [(k_{p_i} + c_{p_i}) + \tau_i(k_{v_i} + c_{v_i})]s + (k_{p_i} + c_{p_i})\tau_i = 0$$

Routh–Hurwitz analysis indicates that for stability, $\tau_i > 0$, and k_i has no bounds because it does not appear in the characteristic equation.

V. Rate-Free Control

Passive filtering can also be used to implement rate-free control laws that do not require rate information for implementation [15,18]. In this case, our motivation is to design a control law that is self-contained (i.e., does not require state information from other vehicles and does not require onboard rate sensing). The derivation begins by redefining the position error of the ith vehicle relative to the reference trajectory.

$$\epsilon_i = x_r - x_i - \sum_{j=1}^{i} \mathrm{d}_j; \quad \dot{\epsilon}_i = \dot{x}_r - \dot{x}_i; \quad \ddot{\epsilon}_i = \ddot{x}_r - \ddot{x}_i = \ddot{x}_r - u_i \tag{24}$$

In addition, the error equations are augmented with a first-order filter of the position error ϵ_i.

$$\dot{\beta}_i = -\tau_i \beta_i + k_i \epsilon_i \tag{25}$$

Lyapunov stability theory [19] was used to determine an appropriate controller to drive the system to its equilibrium state, where error ϵ_i is zero.

$$V(\epsilon_i, \dot{\epsilon}_i, \beta_i) = \frac{\gamma_i}{2}\epsilon_i^2 + \frac{1}{2}\dot{\epsilon}_i^2 + \frac{1}{2}(-\tau_i \beta_i + k_i \epsilon_i)^2 \tag{26}$$

It is easily verified that $V = 0$ at $\epsilon_i = \dot{\epsilon}_i = -\tau_i \beta_i + k_i \epsilon_i = 0$. The design parameter γ_i was added to influence the system performance. The time derivative of Eq. (26) introduces the control input u_i.

$$\begin{aligned} \dot{V}(\epsilon_i, \dot{\epsilon}_i, \beta_i, \dot{\beta}_i) &= \gamma_i \epsilon_i \dot{\epsilon}_i + \dot{\epsilon}_i \ddot{\epsilon}_i + (-\tau_i \beta_i + k_i \epsilon_i)(-\tau_i \dot{\beta}_i + k_i \dot{\epsilon}_i) \\ &= \dot{\epsilon}_i(\gamma_i \epsilon_i + \ddot{x}_r - u_i - k_i \tau_i \beta_i + k_i^2 \epsilon_i) - \tau_i(-\tau_i \beta_i + k_i \epsilon_i)^2 \end{aligned} \tag{27}$$

Stability requires that $\dot{V} \leq 0$, and a control is selected to achieve this result.

$$\begin{aligned} u_i &= (\gamma_i + k_i^2)\epsilon_i - k_i \tau_i \beta_i + \ddot{x}_r \\ &= (\gamma_i + k_i^2)\left(x_r - x_i - \sum_{j=1}^{i} \mathrm{d}_j\right) - k_i \tau_i \beta_i + \ddot{x}_r \end{aligned} \tag{28}$$

We see that u_i requires position x_i, reference x_r, and filter-state β_i information only. This controller development has eliminated the need for rate information in the control input. For this choice of u_i, the first term in Eq. (27) is equal to zero, which leaves

$$\dot{V} = -\tau_i(-\tau_i \beta_i + k_i \epsilon_i)^2 \leq 0$$

The condition $\dot{V} \leq 0$ indicates local stability around the equilibrium states of ϵ_i, $\dot{\epsilon}_i$, and β_i; however, by taking higher derivatives of V, we are able to determine that ϵ_i, $\dot{\epsilon}_i$, and β_i go to zero asymptotically (see the Appendix). This proof of asymptotic stability is an alternative to checking the closed-loop eigenvalues of the state and filter equations.

Whereas the control input does not require rate information, the rates $\dot{x}_i$ must still be estimated to compute the original controls v and ω in Eq. (2). The first-order filter of position used to determine $\dot{\hat{x}}_i$ in the previous section can be implemented here to estimate the rates. The closed-loop rate-free control law augmented with the two first-order filters is shown next. Here, the gains on the position-error filter shown in Eq. (25) are denoted by subscript 1, and the gains on the position filter in Eq. (20) are denoted by subscript 2.

$$\begin{bmatrix} \dot{x}_i \\ \ddot{x}_i \\ \dot{\beta}_i \\ \dot{\phi}_i \end{bmatrix} = \begin{bmatrix} 0 & 1 & 0 & 0 \\ -(\gamma_i + k_{i_1}^2) & 0 & -k_{i_1}\tau_{i_1} & 0 \\ -k_{i_1} & 0 & -\tau_{i_1} & 0 \\ k_{i_2} & 0 & 0 & -\tau_{i_2} \end{bmatrix} \begin{bmatrix} x_i \\ \dot{x}_i \\ \beta_i \\ \phi_i \end{bmatrix} + \begin{bmatrix} 0 & 0 & 0 \\ (\gamma_i + k_{i_1}^2) & 0 & 1 \\ k_{i_1} & 0 & 0 \\ 0 & 0 & 0 \end{bmatrix} \begin{bmatrix} x_r \\ \dot{x}_r \\ \ddot{x}_r \end{bmatrix} + \begin{bmatrix} 0 \\ -(\gamma_i + k_{i_1}^2)\sum_{j=1}^{i} \mathrm{d}_j \\ -k_{i_1}\sum_{j=1}^{i} \mathrm{d}_j \\ 0 \end{bmatrix} \tag{29}$$

Again, the eigenvalues do not have a concise analytical form. Routh–Hurwitz analysis of the characteristic equation

$$\begin{aligned} s^4 + (\tau_{i_1} + \tau_{i_2})s^3 + (\tau_{i_1}\tau_{i_2} + \gamma_i + k_{i_1}^2)s^2 \\ + [(\tau_{i_1} + \tau_{i_2})\gamma_i + \tau_{i_2}k_{i_1}^2)]s + \tau_{i_1}\tau_{i_2}\gamma_i = 0 \end{aligned}$$

becomes quite complicated; however, design parameters may be chosen to satisfy the necessary condition for stability in which all of the coefficients in the characteristic equation must be positive.

VI. Simulation Results

Simulation results are presented here to demonstrate the control-law performance. First, a nondimensional example is presented using the full-state-measurement, rate-estimation, and rate-free control laws presented in Secs. III, IV, and V. Second, simulation results are presented for a formation of UAVs using the full-state measurement control law to demonstrate the applicability of the decentralized formation controller to a realistic UAV application.

A. Nondimensional Simulation Results

The simulation results presented here are intended to demonstrate the performance characteristics of the different formation-control schemes; therefore, the user must appropriately design the control gains and reference trajectory of the formation for a specific vehicle application. All units will be in terms of distance units (DU) and time units (TU) to eliminate any relation to a specific application.

In all simulations in this section, the reference trajectory of the formation from the origin is $x_r = \frac{1}{2}\ddot{x}_r t^2 + \dot{x}_r(0)t$, where $\ddot{x}_r = 1$ and $\dot{x}_r(0) = 0.5$. These values were chosen such that the formation lead vehicle travels one DU in one TU. The desired separation between vehicles in the x and y directions is 0.1 DU.

1. *Full-State Measurement Control*

A five-vehicle formation was simulated for the four gain cases described in Sec. III. Figure 3 shows the (x, y) positions of the vehicles over one TU. Note that the vehicles are traveling from left to right in the figure, and each vehicle has initial position and velocity

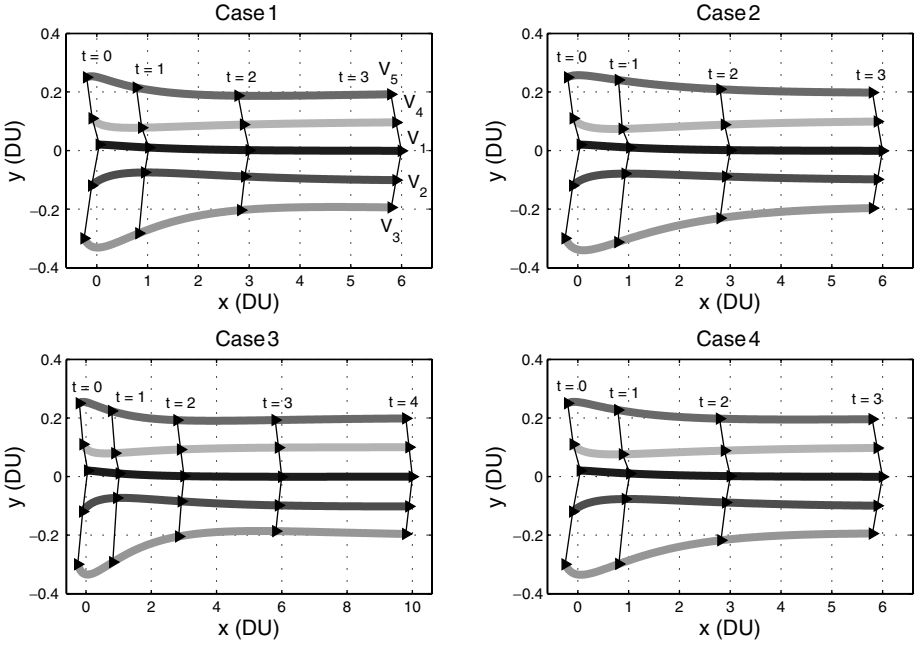

Fig. 3 Simulation results for the general formation-control laws with different gain choices.

errors. The eigenvalues of the characteristic equation were chosen to be equal in all control-gain cases. Although it is difficult to detect in the figure, there are some slight differences in the performance of each control law. These differences are expected, due to the different forms of the closed-loop error dynamics for each gain case. Whereas identical eigenvalues provide the same decay rates for each solution, each gain case has a unique closed-loop form with unique eigenvectors, which leads to variations in the performance of each controller.

Table 1 shows the convergence times for each control law and the minimum separation between vehicle pairs in the formation, in which the desired separation is $\sqrt{2(0.1)^2} = 0.1414$ DU. We have defined the convergence time as the time when the four trailing vehicles are within 10% of their desired separation from their leads. We see that for these gain choices, case 1 provides the fastest convergence and case 3 is the slowest to converge; however, the differences in the table are quite small, and changes to the gains may not result in the same performance trends as those shown here. Further gain tuning could provide desired performance for any of these control choices. Whereas active collision avoidance was not investigated in the control-law design, gain selection and initial vehicle conditions directly affect the aggressiveness of the formation convergence. The gains chosen in this example were selected to provide reasonable separation between the vehicles during convergence. However, in a case of poor initial conditions, the gains could be chosen to make the lead vehicle quickly converge to the reference trajectory, vehicles 2 and 4 less aggressive than the lead, and vehicles 3 and 5 less aggressive than vehicles 2 and 4.

Additionally, the gains used here were selected to limit vehicle accelerations to 1.2 DU/TU^2 (20% greater than the desired acceleration) and to limit angular turn rates to 90 deg/TU. These were arbitrarily chosen limits; however, the gains can be adjusted to achieve any desired acceleration and turn-rate constraints.

2. Rate-Estimation Control

a. Luenberger-Observer Estimation Method. Simulation results were used to evaluate the rate-estimation scheme for initial filter errors in the vehicle rates. The estimation-gain matrices L_i were identical for each vehicle and were chosen such that the state estimators were at least 10 times faster than the closed-loop dynamics. Figure 4 shows one example of the formation convergence (for case 4) with initial-rate inputs to the estimation filter randomly perturbed using a normal distribution with a variance of 0.10 DU/TU. The top plot in Fig. 4 shows (x, y) positions over 5 TU. Formation convergence was achieved in 4.44 TU, with a minimum separation of 0.1210 DU.

Although not necessarily evident in the preceding figure, the commanded velocities and heading angles are highly oscillatory, due to the estimation dynamics from the transformation in Eq. (11). The estimation dynamics induce a phase shift between the estimated and actual vehicle rates, which causes oscillatory behavior of both the estimated and true rates. This behavior is evident in Fig. 5, which shows the separation between vehicle pairs. Despite the oscillatory behavior, the oscillations are lightly damped and the estimated vehicle rates eventually converge to the actual rates. In a practical application, an additional filter of the control commands could reduce the highly oscillatory motion.

One hundred simulations were run for perturbed initial rate estimates with a variance of 0.10 DU/TU. Fifty-five of the simulations converged in an average of 4.21 TU, which indicates that, on average, the formation converges more slowly for estimated rates than when the actual rates are used in the control law. The remaining simulations converged in more than 20 TU, and some of these simulations took as long as 1000 TU to converge using the convergence criteria defined previously. Hence, the transformation in Eq. (11) leads to undesired behavior when rate estimates are determined using a Luenberger observer. In addition, some of the

Table 1 Control-law convergence and minimum-separation results

Case no.	Gains	Convergence time, TU	Minimum separation, DU
1	$k_p, k_v \neq 0$ and $c_p, c_v = 0$	1.99	0.1165
2	$k_p, k_v = 0$ and $c_p, c_v \neq 0$	2.40	0.1247
3	$k_p, k_v, c_v \neq 0$ and $c_p = 0$	3.40	0.1097
4	$k_p, k_v, c_p, c_v \neq 0$	2.08	0.1208

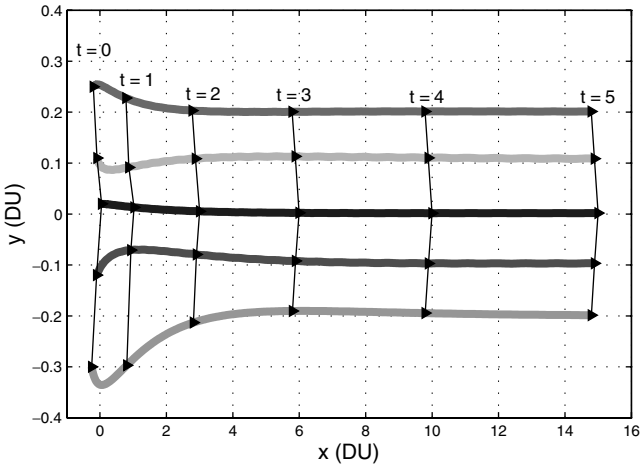

Fig. 4 Simulation results for the Luenberger-observer estimation scheme (case 4).

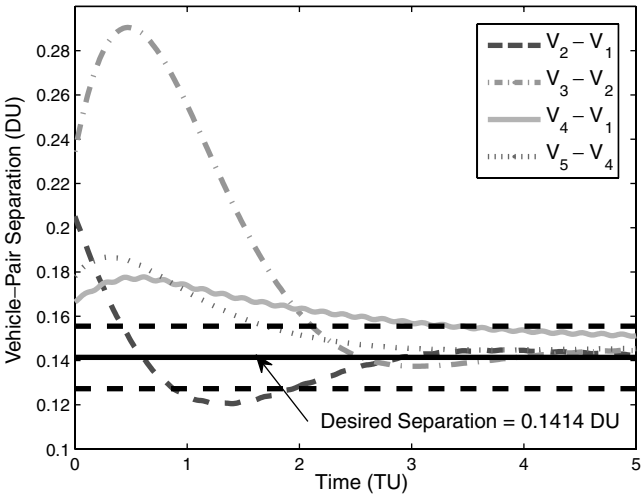

Fig. 5 Vehicle spacing for the Luenberger-observer estimation scheme.

cases violated the acceleration and turn-rate limits, which indicates that the control gains would need to be less aggressive in the rate-estimate case.

b. Passive-Filtering Estimation Method. In the nonlinear-model implementation of the passive filter, the formation stability is sensitive to the initial guesses for ϕ_i. The desired value of $\phi_i(0)$ can be calculated from Eq. (22) and then perturbed by a random error, with some variance to investigate the formation stability around the initial condition for ϕ_i. For a variance of 0.10 DU/TU and $k_i = 5$, the formation does converge to the desired formation; however, there are large oscillations in the vehicle positions, causing the vehicle paths to cross. Improved performance is achieved by increasing k_i to 50. An example of this result is shown in Fig. 6, in which the formation converges to the desired formation in 1.60 TU, with a minimum separation of 0.1396 DU. Over 100 simulations, the average convergence time is 1.50 TU, which means that the passive-filtering technique provides faster convergence for this set of gains than when true rates are known.

In the case that there are no errors on the initial filter states, the value of k_i does not influence the results. However, this gain directly affects the stability and performance of the passive-filter system when there are initial errors in ϕ_i. This result is obvious from Eq. (22), in which larger values of k_i decrease the contribution of ϕ_i in the calculation of $\dot{\hat{x}}_i$. In addition, the passive filter does not display any of the oscillatory behavior that was shown for the Luenberger-observer estimation scheme.

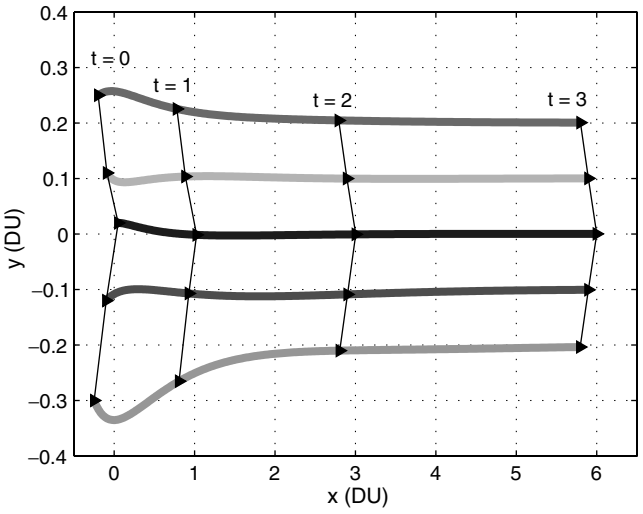

Fig. 6 Simulation results for the passive-filtering estimation scheme (case 4).

3. Rate-Free Control

The rate-free controller performance is demonstrated in Fig. 7 for 5 TU. Here, the gains τ_{i_2} and k_{i_2} remained the same as in the passive-filter implementation, and the gains τ_{i_1}, k_{i_1}, and γ_i were tuned to limit the acceleration and turn rates to the previously specified conditions. In this case, the initial conditions for β_i were set to zero, and the initial conditions for ϕ_i were perturbed from the desired values using a random error. Because of the more sluggish behavior of the rate-free controller, the variance on the errors in $\phi_i(0)$ was increased to 0.50 from 0.10 DU/TU in the previous section. For these conditions, the formation converged in 10.79 TU, with a minimum separation of 0.0862 DU. Out of 100 simulations, all of the initial conditions yielded stable formations, with an average convergence time of 11.41 TU. Vehicle separation is more of a concern with the rate-free controller, due to the lack of state information from other vehicles; therefore, gains must be carefully selected based upon the initial formation to provide adequate separation.

B. UAV Simulation Results

The UCAV6 aircraft model, which is roughly a 60%-scale version of the AV-8B Harrier Aircraft [20,21], was used to simulate a formation of five UAVs. A six-degree-of-freedom state-space aircraft model was obtained by linearizing a nonlinear simulation model about a steady, level, trimmed flight condition (the trim angle of attack is $\alpha_1 = 4.35$ deg, the trim velocity is $V_1 = 128.7$ m/s, the trim elevator deflection is $\delta_{e_1} = 7.5$ deg, and the trim engine thrust is

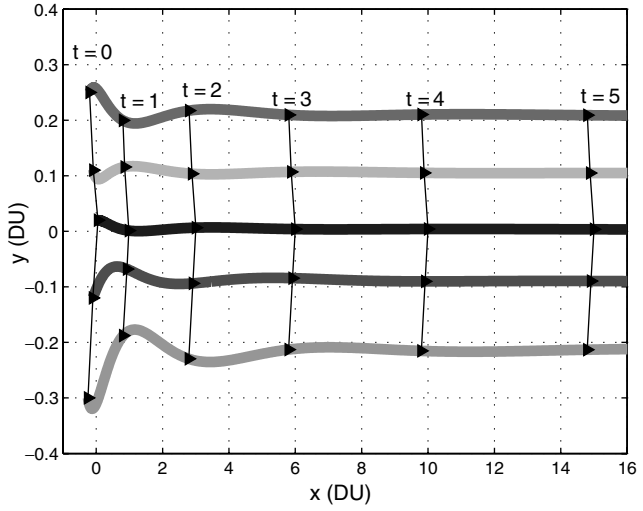

Fig. 7 Simulation results for the rate-free controller (case 4).

55%). The vectors of aircraft states and inputs are shown next.

$$\mathbf{x} = \begin{bmatrix} \delta X & \delta Y & \delta Z & u & v & w & p & q & r & \phi & \theta & \psi \end{bmatrix}^T$$

The states δX, δY, and δZ are perturbations in the aircraft position; u, v, and w are perturbations in the body-fixed velocities; p, q, and r are perturbations in the body-fixed angular velocities; and ϕ, θ, and ψ are Euler angles.

$$\mathbf{u} = \begin{bmatrix} \delta_e & \delta_T & \delta_a & \delta_r \end{bmatrix}^T$$

where δ_a and δ_r are aileron and rudder deflections.

Velocity and heading-angle commands come from the integration of the $\dot{v}$ and ω control inputs, described in Eq. (10), that are determined using the full-state-measurement control law (case 4). An optimal nonzero-set-point controller is then used to steer the aircraft states to track the commanded velocity and heading-angle commands from the formation controller [20,21]. The velocity in the body-fixed y axis is regulated to zero to meet the negligible side-slip assumption from the simplified kinematic model in Eq. (1).

The first vehicle in the formation follows a constant-velocity reference trajectory in the x direction from $(x, y) = (0, 0)$ with $\dot{x}_r = V_1 t$, and the desired separation between vehicles is 100 m in both the x and y directions. Formation results are presented in Fig. 8. The formation converges in 93 s, with a minimum vehicle separation of 137 m. The distances between the vehicle pairs are shown in Fig. 9, in which the vehicles converge to the desired formation from a more widespread initial configuration. Results indicate little overshoot of the desired separation, and thus vehicle collisions are not a concern.

Other state histories are shown in Figs. 10–12. Altitude perturbations are not presented, but deviations were limited to ± 0.2 m from the trim altitude. All perturbed states went to zero, as expected. Formation control and nonzero-set-point gains were selected to limit control-surface deflections, as shown in Fig. 13. All control-surface deflections are reasonable for UAV performance.

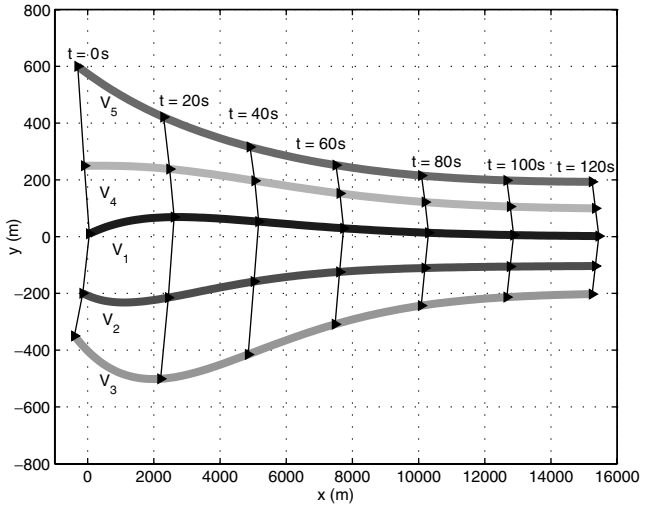

Fig. 8 UAV formation.

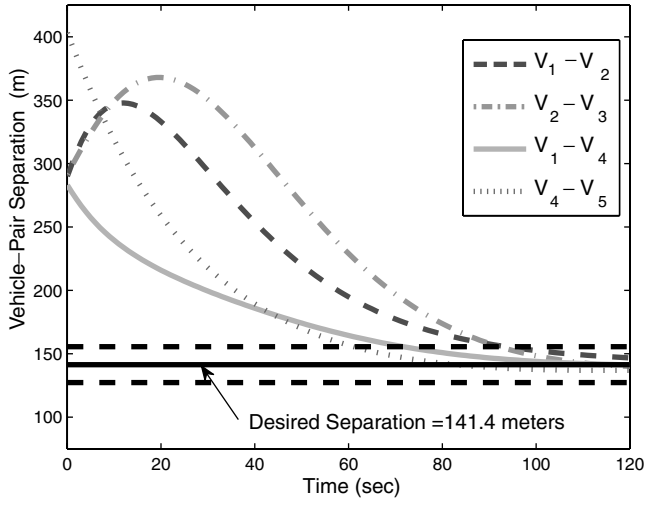

Fig. 9 Separation between vehicle pairs.

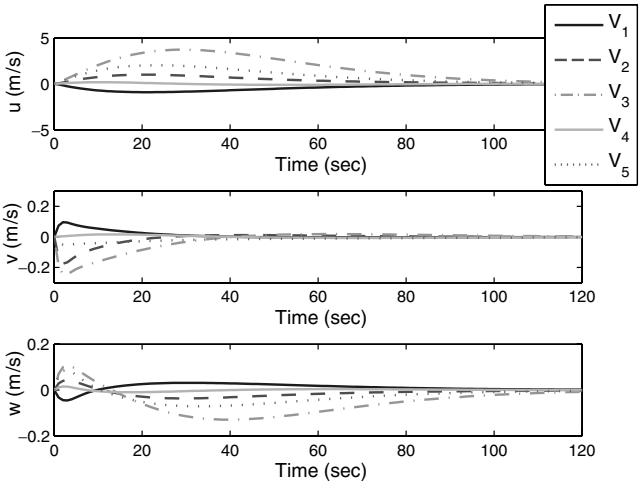

Fig. 10 UAV states: body-fixed velocity perturbations.

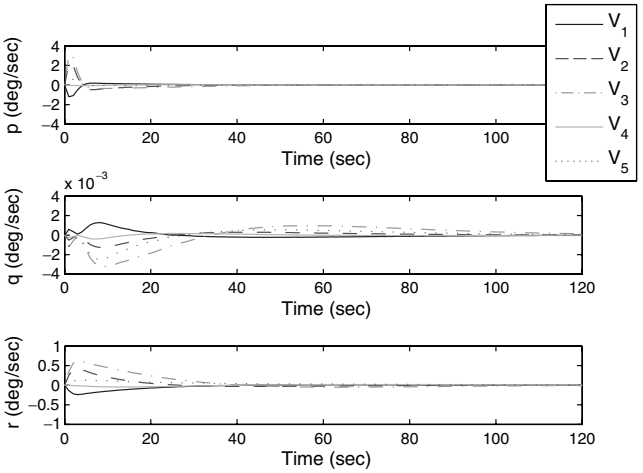

Fig. 11 UAV states: body-fixed angular-velocity perturbations.

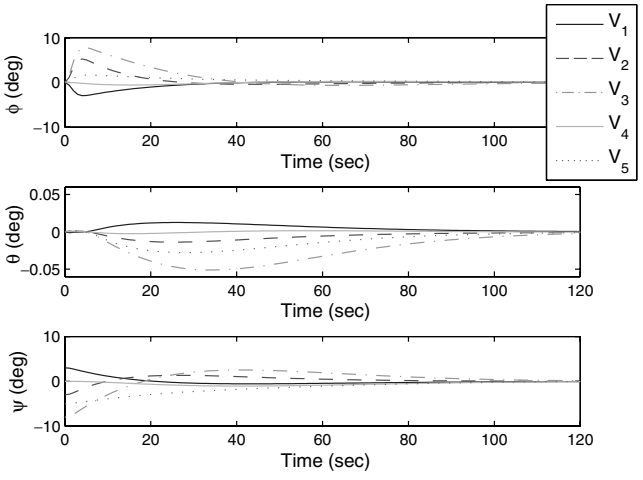

Fig. 12 UAV states: Euler angles.

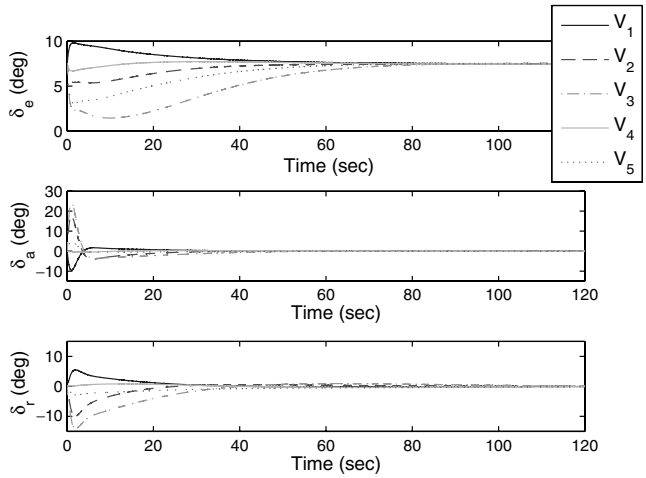

Fig. 13 UAV control-surface deflections.

VII. Conclusions

This paper focused on decentralized cooperative-control design for a multivehicle formation problem in which the vehicles were modeled using a nonlinear, differentially flat, form. Exploiting the differential-flatness properties of the model led to a linear representation of the vehicle model from which position and velocity errors were defined using a leader–follower communication structure. A general control form for an accelerating formation was derived, which contains terms to track both the reference trajectory and the assigned lead-vehicle states. Control gains can be selected to implement a desired tracking strategy and bound control inputs to desired limits.

In addition, two rate-estimation techniques were examined (Luenberger observer and passive filtering) for the case when rate information was not known. Rate estimation provided a challenge in the transformation of the controls in the linear representation to the controls in the nonlinear form. Estimation dynamics influenced the system behavior and were related to the errors between the estimated and actual states. In the rate-estimation case, stability was difficult to quantify. To deal with this challenge, the rate-estimation schemes were designed using the linear model, and simulation results were used to examine stability results. The Luenberger-observer results exhibited oscillatory behavior, due to the rate estimates in the control transformation, whereas the passive filter did not exhibit any oscillatory behavior. In the rate-estimation case, the passive filter is superior to the Luenberger observer in both convergence performance and efficiency.

Finally, a rate-free controller was developed that does not include rate information in the control form. Coupled with the passive filter to estimate vehicle rates, the formation convergence was more sluggish than when rates were included in the control law. However, the sluggish behavior permits greater errors in the initial filter states, thus providing a more robust solution than the Luenberger-observer and passive-filtering schemes when subjected to initial rate-estimation errors. The rate-free control law does not require information from other vehicles in the formation, which can cause concern in vehicle separation; however, gains can be chosen to limit control inputs to provide adequate separation throughout convergence.

Simulation results were presented to demonstrate formation convergence for a nondimensional example using the simple nonlinear model. In addition, simulation results were presented to demonstrate the applicability of the decentralized formation-control law to a six-degree-of-freedom UAV model.

Appendix: Proof of Asymptotic Stability for Rate-Free Control

Junkins and Kim [19] and Mukherjee and Chen [22] explored asymptotic stability for autonomous systems using higher derivatives of the Lyapunov function. The theorem presented in the references states that a sufficient condition for asymptotic stability when $V > 0$ and $\dot{V} \leq 0$ for all states in the region Ω is that the derivatives of V are equal to zero on Z, up to some even order, where Z is the set of points at which $\dot{V}$ is equal to zero, and the first nonzero derivative of V is of odd order and is negative definite for all points on Z. The objective is to prove that $\dot{V}$ is negative definite and $\dot{V} = 0$ for all of the equilibrium points.

The linear equations of motion for the rate-free system are restated next (the vehicle index i was dropped for notational simplicity).

$$\dot{\beta} = -\tau\beta + k\epsilon; \qquad \ddot{\epsilon} = \ddot{x}_r - u \tag{A1}$$

An equilibrium solution of Eq. (A1) is given by $\epsilon = 0$, $\dot{\epsilon} = 0$, and $\beta = 0$. For the Lyapunov function

$$V = \frac{\gamma}{2}\epsilon^2 + \frac{1}{2}\dot{\epsilon}^2 + \frac{1}{2}(-\tau\beta + k\epsilon)^2$$

with $u = (\gamma + k^2)\epsilon - \tau k\beta + \ddot{x}_r$, the time derivative of V was found to be negative semidefinite.

$$\dot{V} = -\tau(-\tau\beta + k\epsilon)^2 \leq 0 \tag{A2}$$

The set Z is defined, where $\dot{V} = 0$.

$$Z = \{\epsilon \in \Re, \dot{\epsilon} \in \Re, (-\tau\beta + k\epsilon) = 0\}$$

The second derivative of V is zero when evaluated on Z, whereas the third derivative is a quadratic function of $\dot{\epsilon}$.

$$\begin{aligned} V^{(3)}|_Z &= -2\tau(-\tau\beta + k\epsilon)(-\tau\ddot{\beta} + k\ddot{\epsilon})|_Z - 2\tau(\tau\dot{\beta} + k\dot{\epsilon})^2|_Z \\ &= -2\tau[\tau(-\tau\beta + k\epsilon) + k\dot{\epsilon}]^2|_Z = -2\tau k^2\dot{\epsilon}^2 \\ &\leq 0 \end{aligned} \tag{A3}$$

Here, it can be seen that $V^{(3)} < 0$ for all $\dot{\epsilon} \neq 0$, but this expression still does not reveal anything about ϵ. A new set is defined,

$$Z_{\text{new}} = \{\epsilon \in \Re, \dot{\epsilon} = 0, (-\tau\beta + k\epsilon) = 0\}$$

such that the third derivative is equal to zero, and higher derivatives of V are taken. The fourth derivative of V is equal to zero when evaluated on Z_{new}, whereas the fifth derivative is a quadratic function of ϵ.

$$\begin{aligned} V^{(5)}|_{Z_{\text{new}}} &= -4\tau k^2[\ddot{\epsilon}^2 + \dot{\epsilon}\epsilon^{(3)}]|_{Z_{\text{new}}} \\ &= -4\tau k^2(\ddot{x}_r - u)^2|_{Z_{\text{new}}} \\ &= -4\tau k^2[\ddot{x}_r - (\gamma + k^2)\epsilon + \tau k\beta - \ddot{x}_r]^2|_{Z_{\text{new}}} \\ &= -4\tau k^2[-(\gamma + k^2)\epsilon + k(k\epsilon)]^2|_{Z_{\text{new}}} \\ &= -4\tau k^2(-\gamma\epsilon)^2 < 0 \quad \forall\ \epsilon \neq 0 \end{aligned} \tag{A4}$$

From Eq. (A4), which is an odd, nonzero derivative of V, we can conclude that $\dot{V} = 0$ only at the equilibrium points: ϵ, $\dot{\epsilon}$, and $\beta = 0$. Therefore, $\dot{V}$ is negative definite, which implies that ϵ, $\dot{\epsilon}$, and β asymptotically approach their equilibrium points.

Acknowledgments

Research funding was provided by the National Science Foundation Graduate Research Fellowship. Any opinions, findings, conclusions, or recommendations expressed in this document are those of the authors and do not necessarily reflect the views of the National Science Foundation. The authors would like to thank James Doebbler for his assistance with the UAV simulation and the reviewers for their valuable, insightful comments.

References

[1] Siljak, D. D., *Decentralized Control of Complex Systems*, Academic Press, New York, 1991, Chap. 9.

[2] Feddema, J. T., Lewis, C., and Schoenwald, D. A., "Decentralized Control of Cooperative Robotic Vehicles: Theory and Application," *IEEE Transactions on Robotics and Automation*, Vol. 18, No. 5, 2002,

pp. 852–864.
doi:10.1109/TRA.2002.803466

[3] Caicedo, R., Valasek, J., and Junkins, J., "Preliminary Results of Vehicle Formation Control Using Dynamic Inversion," AIAA Aerospace Sciences Meeting and Exhibit, Reno, NV, AIAA Paper 2004-0295Jan. 2004.

[4] Olfati-Saber, R., and Murray, R., "Distributed Cooperative Control of Multiple Vehicle Formations Using Structural Potential Functions," *15th IFAC World Congress* [CD-ROM], Elsevier, New York, 2003.

[5] Siljak, D. D., *Large-Scale Dynamic Systems: Stability and Structure*, Springer, New York, 1978, Chap. 3.

[6] Ikeda, M., Siljak, D. D., and White, D. E., "Decentralized Control with Overlapping Information Sets," *Journal of Optimization Theory and Applications*, Vol. 34, No. 2, 1981, pp. 279–310.
doi:10.1007/BF00935477

[7] İftar, A., and Özgüner, U., "Contractible Controller Design and Optimal Control with State and Input Inclusion," *Automatica*, Vol. 26, No. 3, 1990, pp. 593–597.
doi:10.1016/0005-1098(90)90031-C

[8] Stipanović, D. M., İnalhan, G., Teo, R., and Tomlin, C. J., "Decentralized Overlapping Control of a Formation of Unmanned Aerial Vehicles," *Automatica*, Vol. 40, Aug. 2004, pp. 1285–1296.
doi:10.1016/j.automatica.2004.02.017

[9] Pledgie, S. T., Hao, Y., Ferreira, A. M., Agrawal, S. K., and Murphey, R., "Groups of Unmanned Vehicles: Differential Flatness, Trajectory Planning, and Control," *Proceedings of the 2002 IEEE International Conference on Robotics and Automation*, Inst. of Electrical and Electronics Engineers, Piscataway, NJ, 2002.

[10] Altafini, C., "General *n*-Trailer, Differential Flatness and Equivalence," *Proceedings of the 38th IEEE Conference on Decision and Control*, Vol. 3, Inst. of Electrical and Electronics Engineers, Piscataway, NJ, 1999, pp. 2144–2149.

[11] Lećhevin, N., and Rabbath, C. A., "Sampled-Data Control of a Class of Nonlinear Flat Systems with Application to Unicycle Trajectory Tracking," *Transactions of the ASME*, Vol. 128, No. 3, 2006, pp. 722–728.
doi:10.1115/1.2234491

[12] Murray, R. M., Rathinam, M., and Sluis, W., "Differential Flatness of Mechanical Control Systems: A Catalog of Prototype Systems," *Proceedings of the 1995 ASME International Mechanical Engineering Congress and Expo*, American Society of Mechanical Engineers, New York, 1995, pp. 349–357.

[13] Nieuwstadt, M. V., Rathinam, M., and Murray, R., "Differential Flatness and Absolute Equivalence," *Proceedings of the 33rd IEEE Conference on Decision and Control*, Vol. 1, Inst. of Electrical and Electronics Engineers, Piscataway, NJ, 1994, pp. 326–332.

[14] Chen, C.-T., *Linear System Theory and Design*, Oxford Univ. Press, New York, 1999, Chap. 8, Section4.

[15] Berghuis, H., and Nijmeijer, H., "Global Regulation of Robots Using Only Position Measurements," *Systems and Control Letters*, Vol. 21, No. 4, 1993, pp. 289–293.
doi:10.1016/0167-6911(93)90071-D

[16] Subbarao, K., and Akella, M. R., "Differentiator-Free Nonlinear Proportional-Integral Controllers for Rigid-Body Attitude Stabilization," *Journal of Guidance, Control, and Dynamics*, Vol. 27, No. 6, 2004, pp. 1092–1096.
doi:10.2514/1.8366

[17] Azor, R., Bar-Itzhack, I. Y., and Harman, R. R., "Satellite Angular Rate Estimation from Vector Measurements," *Journal of Guidance, Control, and Dynamics*, Vol. 21, No. 3, 1998, pp. 450–457.

[18] Akella, M. R., "Rigid Body Attitude Tracking without Angular Velocity Feedback," *Systems and Control Letters*, Vol. 42, No. 4, 2001, pp. 321–326.
doi:10.1016/S0167-6911(00)00102-X

[19] Junkins, J. L., and Kim, Y., *Introduction to Dynamics and Control of Flexible Structures*, AIAA, Washington, D.C., 1993, Chap. 3.

[20] Tandale, M., Bowers, R., and Valasek, J., "Trajectory Tracking Controller for Vision-Based Probe and Drogue Autonomous Aerial Refueling," *Journal of Guidance, Control, and Dynamics*, Vol. 29, No. 4, 2006.

[21] Doebbler, J., Spaeth, T., Valasek, J., Monda, M. J., and Schaub, H., "Boom and Receptacle Autonomous Air Refueling Using Visual Snake Optical Sensor," *Journal of Guidance, Control, and Dynamics*, Vol. 30, No. 6, 2007.

[22] Mukherjee, R., and Chen, D., "Asymptotic Stability Theorem for Autonomous Systems," *Journal of Guidance, Control, and Dynamics*, Vol. 16, No. 5, 1993, pp. 961–963.